Supporting information:

Fabrication of reversible SnS$_2$/RGO nanocomposite for high

performance lithium storage

Shancheng Yan, Keyu Li, Zixia Lin, Haizeng Song, Tian Jiang, Jiansheng Wu, Yi Shi
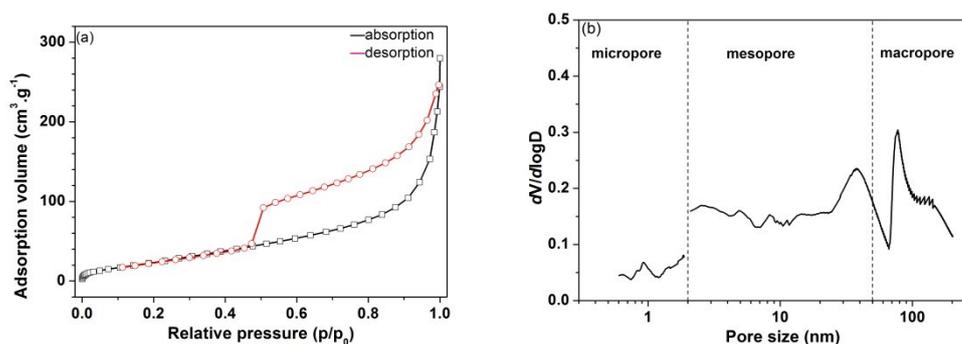
Fig. S1 (a) N$_2$ adsorption/desorption isotherm of the SnS$_2$/RGO nanocomposites synthesized for 24h; (b) Pore size distribution calculated from the absorption branch.
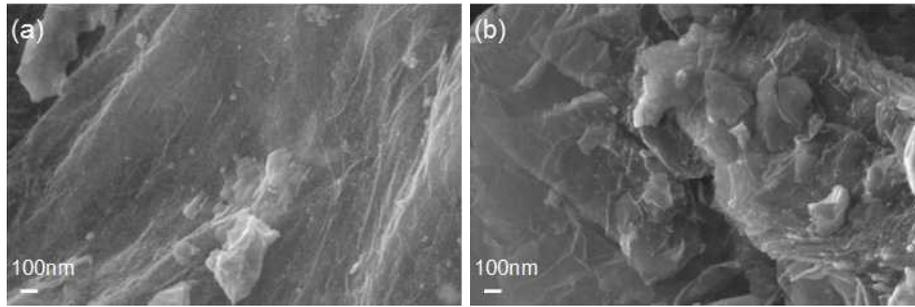
Fig. S2 SEM images of SnS$_2$/RGO nanocomposites synthesized using different solvents: (a) H$_2$O and (b) ethanol.

It has been found that the solvent is a vital factor in controlling the morphology of SnS$_2$/RGO compound. Fig. S2 shows the observations in the morphologies of SnS$_2$/RGO synthesized in water and ethanol solvent systems with other conditions unchanged. Only very small amounts of irregular SnS$_2$ nanoparticles are observed on the thicker RGO nanosheets when the solvents are changed as H$_2$O and ethanol. These experimental results demonstrate that the morphologies of SnS$_2$/RGO nanostructures are sensitive to the solvent used in solvothermal synthesis. It is proposed that the –OH groups of ethylene glycol may lead to changes in the surface energies of SnS$_2$ and RGO by forming chemical bonds between the surface Sn atoms of SnS$_2$ nanoparticles and the oxygen-containing groups on the RGO surface, which, corresponding to observations in FTIR and Raman spectroscopy, may be responsible for the formation of SnS$_2$/RGO nanostructures.[14, 29]
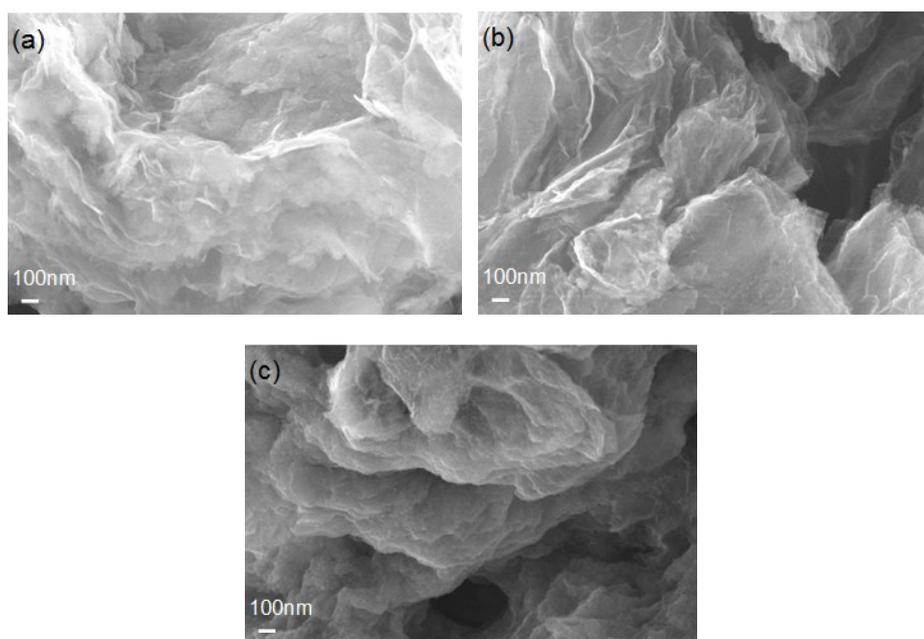
Fig. S3 SEM images of SnS$_2$/RGO nanocomposites synthesized at different mass ratios of RGO/SnCl$_4\cdot$5H$_2$O: (a) 1:3, (b) 1:4, and (c) 1:6.

We also carried out experiments to study the influence of varying the mass ratio of RGO and SnCl$_4\cdot$5H$_2$O on the product morphology. As shown in Fig. S3, the mass ratio of RGO/SnCl$_4\cdot$5H$_2$O plays a significant role in the formation of different product structures. SnS$_2$ particles aggregate to form into big particles on the surface of RGO nanosheets in Fig. S3a. When the mass ratio of RGO/SnCl$_4\cdot$5H$_2$O is 1:4, only a few of the nanoparticles disappeared on irregular RGO nanosheets (Fig. S3b). SnS$_2$ particles are found to be distributed uniformly, while RGO nanosheets pile into large pieces (Fig. S3c). The structure may have the disadvantage of lithium ions diffusion and may reduce the conductivity used as anodes for lithium ion batteries.
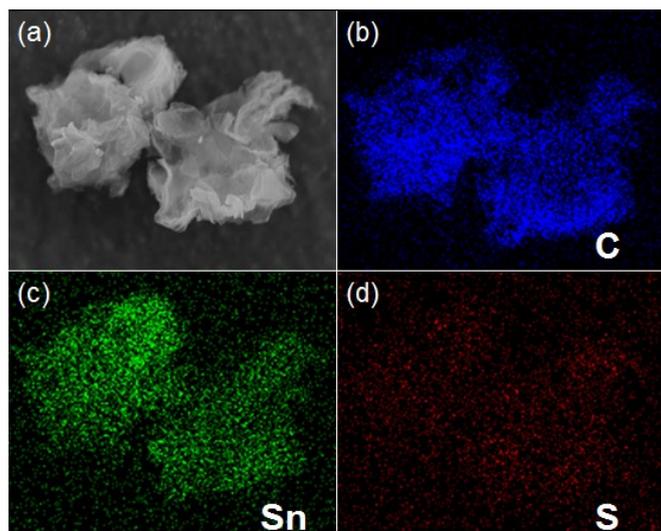
Fig. S4 EDX mapping images of the SnS$_2$/RGO with corresponding SEM image.
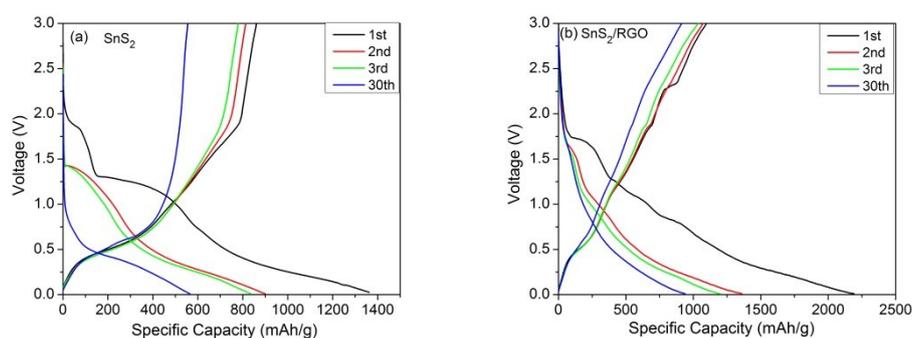
Fig. S5 (a) SnS_2 and (b) SnS_2/RGO Discharge/charge voltage profiles of SnS_2 anode at a current of 0.1 A/g.

Fig. S 5a and Fig. S 5b shows a higher initial capacity of 2190.5 mAhg[-1] for SnS_2/RGO anode as compared to the initial capacity of 1382.4 mAhg[-1] for SnS_2, achieved at a current of 0.1 A/g. Even after 30 cycles, the discharge capacity value of about 939.9 mAhg[-1] of SnS_2/RGO architecture is nearly twice as large as the value for SnS_2 (564.6 mAhg[-1]), which can be ascribed to a highly conductive network of RGO nanosheets.
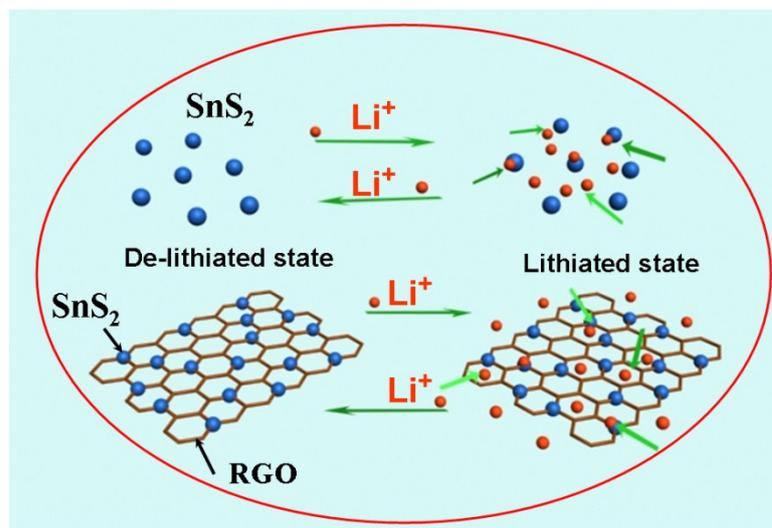
Scheme S1. Schematic illustration of SnS_2 nanoparticles and SnS_2/RGO nanocomposites during lithium ion insertion and extraction.
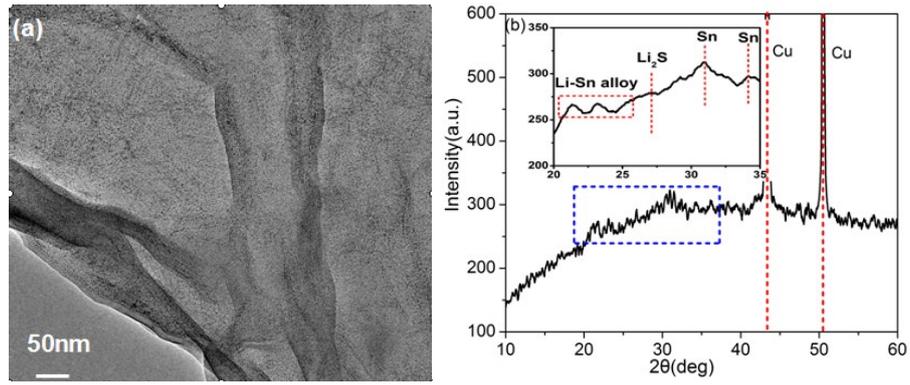
Fig. S6 (a) TEM image in the presence of carbon black and PVDF binders of the

cycled electrode, (b) XRD of SnS$_2$/RGO electrode after charge-discharge cycles.